Measurement Uncertainties in *I–V* Calibration of Multi-junction Solar Cells for Different Solar Simulators and Reference Devices

S. Kasimir Reichmuth , Gerald Siefer, Michael Schachtner, Matthias Mühleis, Jochen Hohl-Ebinger, and Stefan W. Glunz

Abstract—Different types of dual-junction solar cells (perovskite/silicon and GaInP/(Al)GaAs) are used in an investigation of measurement uncertainty for electrical characterization of multi-junction solar cells. A method traceable to international reference standards is presented. The spectral mismatch factor matrix is introduced and used with a Monte-Carlo method including manifold correlated and uncorrelated uncertainties. In this way, a detailed analysis of the solar simulator's spectral irradiance and its influence on uncertainty becomes possible. The use of subcell-adapted and broadband reference solar cells is addressed regarding their impact on uncertainty. This allows for finding optimal conditions for calibration with lowest measurement uncertainty. The short-circuit current of a series connected multi-junction solar cell is affected by luminescence coupling and other effects. With an experimental method it is shown how the uncertainty of the device short-circuit current can be precisely determined. The spectrometric characterization method allows deriving uncertainties of all *I–V* parameters. In this way a complete evaluation of measurement uncertainty for the calibration of multi-junction solar cells at standard testing conditions is introduced. This article is an extension to our work presented at the 46th IEEE PVSC. Here, we have added a detailed analysis of the influence of different solar simulator spectral irradiance distributions on measurement uncertainty by evaluating a Monte Carlo simulation introducing correlation coefficients. In addition for the first time, it is shown how luminescent coupling influences the calibration of multi-junction solar cells and how the effect needs to be implemented into the uncertainty of measurement for the short-circuit current as well as efficiency.

Index Terms—Calibration, III–V semiconductor materials, measurement uncertainty, Monte Carlo methods, multi-junction devices, Perovskite semiconductor materials, photovoltaic cells.

I. INTRODUCTION

AT PRESENT, the market in photovoltaic solar energy conversion is mainly driven by single-junction, silicon-based solar cells. These state-of-the-art photovoltaic devices are close to reaching their physical conversion limit [2]. To further increase efficiency new technologies based on tandem structures are investigated [3], [4]. At the moment, different material combinations (perovskite on Si, III–V on Si and others) are in the focus of research [5]. A precise and accurate efficiency measurement of such devices is thus a crucial part for a world-wide reproducible comparison of solar cell performance in R&D and industry.

For a traceable calibration of solar cells according to ISO 17025 [6], the equipment used needs to be well understood, and its components, its uncertainties and measurement procedures have to be considered.

A central issue for lowering the uncertainty in measurement are reference materials such as reference solar cells [7] and standard lamps. These are typically provided with their specific uncertainty by national metrological institutes and are used for calibrating the irradiance of the solar simulator and the spectro-radiometer used for the measurement of the spectral distribution of the solar simulator.

While there is some literature on the correct measurement of multi-junction solar cells, publications on traceable measurement uncertainties for the characterization of those is scarce. Yet, uncertainties in measurement for series connected multi-junction solar cells need to be determined in another way than those for single-junction solar cells. This article describes the effort at CalLab PV Cells (Fraunhofer ISE) to improve its capability to calibrate multi-junction solar cells.

Within this work a general method traceable to SI (International System of Units) is proposed, which quantifies uncertainties in measurement of multi-junction devices under synthetic solar simulator spectra. Exemplarily, the influence of using different types of reference cells is assessed within a Monte Carlo simulation for two spectrally different solar simulators. While the uncertainty of the spectral mismatch of multi-junction solar cells is calculated with the respective data of a dual-junction

S. Kasimir Reichmuth, Gerald Siefer, Michael Schachtner, Matthias Mühleis, and Jochen Hohl-Ebinger are with the Fraunhofer Institute for Solar Energy Systems ISE, Heidenhofstraße 2, 79110, Freiburg, Germany (e-mail: kasimir.reichmuth@ise.fraunhofer.de; gerald.siefer@ise.fraunhofer.de; michael.schachtner@ise.fraunhofer.de; matthias.muehleis@ise.fraunhofer.de; jochen.hohl-ebinger@ise.fraunhofer.de).

Stefan W. Glunz is with the Fraunhofer Institute for Solar Energy Systems ISE 79110, Freiburg, Germany, and also with the Laboratory for Photovoltaic Energy Conversion, University of Freiburg 79085, Freiburg, Germany (e-mail: stefan.glunz@ise.fraunhofer.de).

Color versions of one or more of the figures in this article are available online at https://ieeexplore.ieee.org.

Digital Object Identifier 10.1109/JPHOTOV.2020.2989144

perovskite/silicon solar cell (Oxford PV/Oxford/Helmholtz), the influence of luminescent coupling (LC) on the uncertainty of the device's current-voltage parameters is elaborated with spectrometric characterization performed on two dual-junction III–V cells (GaInP/GaAs and GaInP/AlGaAs) (Fraunhofer ISE).

II. Measurement Uncertainties in Multi-junction Device *I–V* Characterization

In the following sections, we discuss the uncertainties in multi-junction solar cell current-voltage (*I–V*) measurements following a calibration sequence. Typically, component cells (also called "isotype cells") spectrally matched to the subcells of the corresponding multi-junction solar cell are used for setting the spectral irradiance of the solar simulator. As the available component cells, however, often do not perfectly match the spectral responsivity of the subcells of the multi-junction solar cell, it is beneficial to introduce a generalized spectral mismatch correction procedure. First the measured spectral responsivity with its respective measurement uncertainty of the multi-junction device under test is used to set the solar simulator to the required (relative) spectral irradiance distribution. Reference solar cells are then used to set the irradiance [8], [9]. This enables electrical characterization at reference conditions.

The spectral responsivity of solar cells is a useful quantity to calculate currents generated under incident spectral irradiance distributions. For better graphical observation, it can be translated into the external quantum efficiency (EQE), showing how successful incident photons impinging on the solar cell generate current at each wavelength. Therefore, we use the quantity EQE in the figures.

The determination of uncertainty for the short-circuit current of multi-junction devices is not straight forward. Due to the series connection, the subcell generating the least current will limit the overall current of the device. The limiting subcell is therefore forced to operate under reverse bias. The resulting device's short-circuit current (I_{sc}) may deviate from the limiting short-circuit current of the limiting subcell ($I_{sc-TC, i}$), as it can be strongly influenced by different effects. LC from subcells with higher [10] or same bandgap [11] effectively increases the overall device current and performance. For the case of a low parallel resistance (R_p) [12] of the limiting subcell, or when the limiting subcell is forced to operate in reverse-bias breakdown (RBB) [13], the device I_{sc} will deviate from $I_{sc-TC, i}$ as well, but will operate with lower fillfactor and thus performance. Therefore, also the uncertainty of the device short circuit current will in the cases of LC, R_p, and RBB deviate from the uncertainty of the limiting subcell.

In the following Section A, it is discussed how the uncertainties of the short-circuit current of each subcell of the device under test can be determined and traced back to primary calibrated reference solar cells and standard lamps. In Section B, the deviation of the device's I_{sc} from the short-circuit current of the limiting subcell and the influence on its respective uncertainty is examined. Last, in Section C, a method for extracting the uncertainty of the other *I–V* parameters of the device is presented. In this article, we have used capital letters for quantities in absolute units whereas we have used small letters for relative quantities.

A. Uncertainties of Multi-Junction Device Subcell Short-Circuit Current u($I_{sc-TC, i}$)

For a proper calibration of a multi-junction solar cell, the measurement procedure needs to follow a different routine than for single-junction solar cells. Here, the solar simulator is set in a way that each subcell "*i*" of the test sample (TC_i) generates the same short-circuit current ($I_{sc-TC, i}$) under the simulator spectral irradiance (Sim) as it would do under the reference spectral irradiance (Ref). To fulfill the condition

$$I_{sc-TC,i}^{Ref} = I_{sc-TC,i}^{Sim} \tag{1}$$

for various kinds of multi-junction cells, a *spectrally* tunable solar simulator is mandatory, whereas for single-junction solar cells a single broadband light source adjustable only in irradiance is sufficient. Different approaches to realize this requirement exist and are described in literature [8], [14]–[18].

The uncertainty of the short-circuit current of each subcell under test can be formulated by extending the above equation with the terms necessary for simulator calibration. The resulting eq. (2) contains different additional input quantities subject to uncertainty and represents the model equation according to the international standard "Guide to the Expression of Uncertainty in Measurement" (GUM) [19]. This equation reflects the metrological traceability throughout the calibration chain. The uncertainties of $I_{sc-TC, i}$ can be related to SI units, by taking into account the primary calibrated reference solar cell and the terms that during calibration cause deviation from reference conditions such as the simulator spectral irradiance, the spectral mismatch between reference and test solar cell, etc. The abbreviations are: "RC $_j$": reference cell "*j*", *u*: uncertainty, SMM_{ij}: spectral mismatch matrix element [see (3)], $f_{1...x}$: correction factors (explained below). The terms of (2) are relating to uncertainties from a) electrical measurement of the test and reference cells, b) primary calibration of the reference cell c) spectral mismatch matrix element SMM_{ij} (details in the following), and d) other setup related correction factors "*f*", such as sample positioning, height, temperature, beam divergence, temporal stability of relative spectral distribution of irradiance and others. Obviously, the measurement procedure aims at setting the equipment in a way that the value of each "*f*" should reach "1" [19]. Nevertheless, their specific uncertainty is not zero, so that they need to be incorporated in the equation.

$$I_{sc-TC\,i}^{Ref} = \underbrace{\frac{\overbrace{I_{sc-TC\,i}^{Sim}}^{a)\ u:\ \text{electrical measurement}}}{I_{sc-RC\,j}^{Sim}}}_{c)\ u:\ \text{simulator irradiance}\ u:\ \text{SR measurement}} \cdot \frac{\overbrace{I_{sc-RC\,j}^{Ref}}^{b)\ u:\ \text{primary calibration}}}{SMM_{ij}} \cdot \underbrace{f_1 \cdot f_2 \cdots f_x}_{d)\ u:\ \text{setup related}} \tag{2}$$

As an indication, including the different uncertainties from a), b), c), and d) into the uncertainty budget, an expanded uncertainty ($k = 2$) as low as 1.5…2.0 % for the short-circuit current of multi-junction solar cells can be reached at present. Such low values for uncertainty, however, need to follow very strict and regular in depth assessment of advanced equipment as required for accredited calibration laboratories.

The spectral mismatch element SMM_{ij} is defined in (3). In analogy to the spectral mismatch factor in single-junction measurement [20], [21], it requires only relative spectral responsivity and relative spectral irradiance data and is extended for multi-junction solar cells to a matrix. Each single element (SMM_{ij}) of the matrix takes into account the spectral mismatch of the respective subcell under test to a specific reference solar cell considering the reference solar spectral irradiance and the solar simulator spectral irradiance. The abbreviations are as follows: SMM_{ij}: spectral mismatch matrix element, sr_j^{RC}: relative spectral responsivity of jth reference cell, sr_i^{TC}: relative spectral responsivity of the ith test subcell, e^{Ref}, e^{Sim}: relative spectral irradiance of reference and simulator spectrum.

$$SMM_{ij} = \frac{\int sr_j^{RC}(\lambda)\, e^{Ref}(\lambda)\, d\lambda}{\int sr_j^{RC}(\lambda)\, e^{Sim}(\lambda)\, d\lambda} \cdot \frac{\int sr_i^{TC}(\lambda)\, e^{Sim}(\lambda)\, d\lambda}{\int sr_i^{TC}(\lambda)\, e^{Ref}(\lambda)\, d\lambda}$$
(3)

Evaluating the influence of different solar simulator spectral irradiance distributions and reference solar cells

The above set of equations is a useful tool for finding optimal settings in calibration in respect to lowest uncertainties in measurement. For solar simulators with spectral distributions close to the reference spectral irradiance, the use of solely the SMM for quality assessment is not adequate, as both fraction terms in (3) will have values close to unity, independent of the difference between sr^{TC} and sr^{RC}. Uncertainties of the spectral irradiance distribution of solar simulators, however, vary in dependence of wavelength. This is especially true for multisource simulators. Consequently, it can be clearly concluded, that the mismatch factor itself is a poor indicator for the quality of measurement, and that instead its uncertainty should be considered [22].

In the following, we evaluate the influence on uncertainty of two different designs of solar simulator spectral irradiance distributions and reference solar cells, by calculating the uncertainty of the respective SMM_{ij} when calibrating a dual-junction perovskite/Si test sample from Oxford PV/Oxford/Helmholtz [23].

Fig. 1 shows the EQE of tested subcells and reference cells, the spectral irradiance distribution of two dual light source simulators composed of Xenon and Halogen lamps. The two simulators are designed by filtering Xenon arc and Halogen incandescent light sources either by clear spectral separation (simulator 1), or by overlapping two lamp spectral distributions (simulator 2). The separate peaks in the irradiance distribution of the Halogen light of simulator 2 are caused by two dichroic mirrors serving as spectral filters and optical beam guide [24]. The reference solar cells used here are a broadband and two filtered—and thus more subcell adapted—Silicon reference solar cells in WPVS housing [7]. The filters are part of the encapsulation.

The quantitative investigation of the uncertainty of the SMM is based on a Monte Carlo method and expands earlier work [22], [25]. Here, a more complex approach including wavelength dependent correlations [26]–[28] is implemented, where the input uncertainties may be statistically linked to other wavelength regions. This corresponds to realistic behavior in measurement. Potential sources for wavelength correlated uncertainties are irradiance fluctuations of light sources, bandwidth of and stray
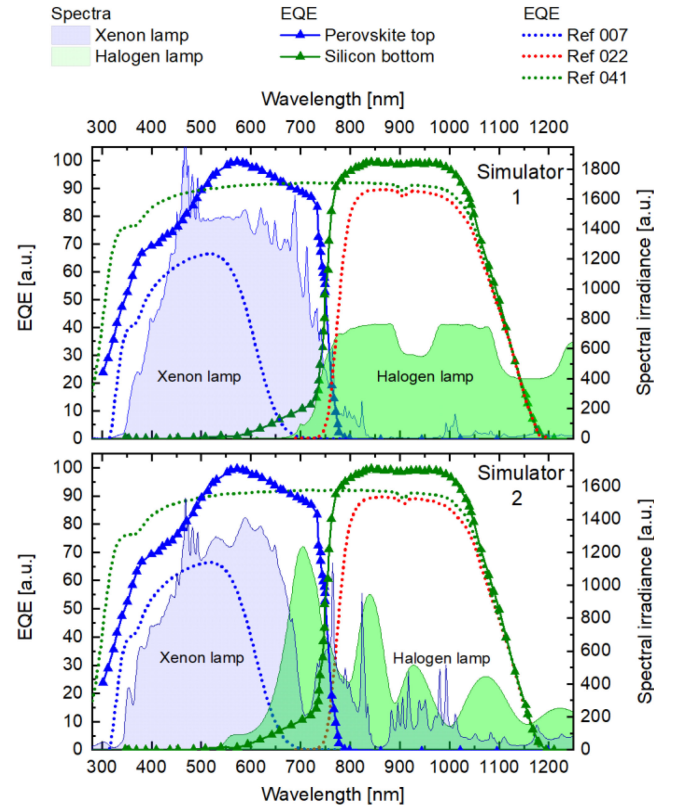

Fig. 1: EQE of a dual-junction perovskite/Si sample (Oxford PV/Oxford/Helmholtz) as triangles, EQE of three reference solar cells as dotted lines and spectral irradiance distributions of two different solar simulators (spectra shown as filled areas).

light in the spectroradiometer, spectrally selective reflections in the optical paths, wavelength dependent stray light contributions in the simulator, and etc. If wavelength correlation would not be accounted for, the calculated uncertainty would indeed be lower, but faulty.

The Monte Carlo simulation calculates (3) for a set of random variations of its elements, where all input quantities are associated with a specific uncertainty except for the reference spectral irradiance e^{Ref}, which is a set of data without uncertainty defined by an international standard [29]. The mean value of all Monte Carlo runs of (3) defines the respective spectral mismatch element SMM_{ij} of the matrix. The standard deviation in turn defines its relative uncertainty $u(SMM_{ij})$.

We calculated the $u(SMM_{ij})$ for two distinct cases to evaluate the influence of different input uncertainties on the result. Case 1 accounts for uncertainties of equipment in use in the calibration laboratory of Fraunhofer ISE. This is a case representing rather low uncertainties. We have defined a case 2 for comparison with uncertainties deriving from more standard measurement equipment. The instability of the simulator lamps was defined by the minimal requirement for a class A+ simulator as discussed for the new standard 60904-9 [30]. For resolution and bandwidth of the spectroradiometer for case 2, we consulted the datasheet of a compact Zeiss diode array-based tool, representing a reproducible industry standard. The correlated uncertainties considered are listed in Table II in the Appendix.
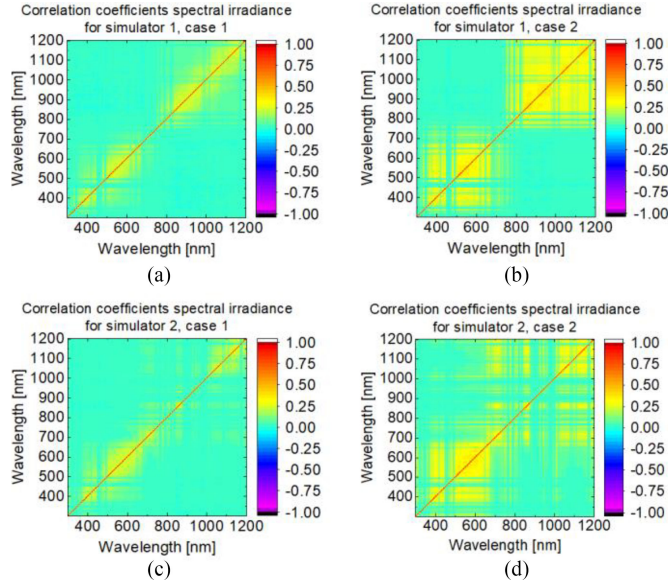
Fig. 2: Plots of correlation coefficients obtained from the covariance matrix of spectral irradiance values of two solar simulators. For better visibility the bandwidth uncertainty is set to be uncorrelated. (a): Case 1, simulator 1; (c): Case 1, simulator 2; (b): Case 2, simulator 1; (d): Case 2, simulator 2. Case 1: low calibration laboratory uncertainties. Case 2: calculations with higher uncertainties.

The quantities describing spectral responsivity of reference and test cells were attributed globally with 50% uncorrelated and 50% wavelength correlated uncertainty as we focused the work on different solar simulator spectral irradiance distributions.

One insight of the Monte Carlo simulation is the distribution of wavelength correlated uncertainty of the solar simulator spectra. The four plots in Fig. 2 show the correlation coefficient matrices of the spectral irradiance of the two solar simulators for both cases. They indicate how light with a certain wavelength of the simulator spectral irradiance distribution is correlated to light of other wavelengths. When comparing solar simulators with similar uncertainty contributions in the spectral irradiance the total uncertainty will be lower for correlation coefficients close to zero.

Here, for better visibility of the plots the uncertainties of the spectroradiometer bandwidth is set to be uncorrelated, as it would otherwise dominate the graphics, but is practically affecting uncertainty mainly where steep changes of spectral responsivity take place. For the calculation of the $u(\mathrm{SMM}_{ij})$ and all other results in Table I, it is obviously considered.

In case 1 for both simulators only slight positive correlation is notable [Fig. 2(a), (c)]. It is centered close around the diagonal with only little range. For case 2, the plots show a completely different distribution of the correlation coefficients [Fig. 2(b), (d)]. For simulator 1 in (b) a clear separation of partly correlated and uncorrelated coefficients is visible. The uncertainty of the spectral irradiance shows correlation only to wavelengths within the spectral band of the respective lamp, whereas there is almost no correlation to the band of the other lamp. At single wavelengths corresponding to peak values in the spectral irradiance distribution narrow green lines show deviations from the positive correlation of the yellow areal-like distribution around them. These lines correspond to the (uncorrelated) bandwidth

TABLE I
UNCERTAINTY MATRIX OF THE SPECTRAL MISMATCH – CASE 1

Solar Simulator 1	Reference Cells		
	Subcell adapted		Broadband
	Ref007	Ref022	Ref041
Perovskite Top	0.20 % (1.0037)	0.63 % (0.9753)	0.29 % (0.9990)
Silicon Bottom	0.64 % (1.0037)	0.12 % (0.9752)	0.30 % (0.9990)
Solar Simulator 2	**Reference Cells**		
	Subcell adapted		Broadband
	Ref007	Ref022	Ref041
Perovskite Top	0.23 % (1.1795)	0.47 % (1.0527)	0.22 % (1.0083)
Silicon Bottom	0.56 % (1.1794)	0.12 % (1.0526)	0.23 % (1.0082)

Case 1. Relative uncertainties of the spectral mismatch $u(SMM_{ij})$ for dual-junction perovskite/silicon test device (Oxford PV/Oxford/Helmholtz) and the subcell adapted and broadband reference cells at both solar simulators. $k = 2$ The spectral mismatch value SMM_{ij} is given in brackets. 100.000 Monte Carlo draws. Reference cells are named according to Fig. 1.

uncertainty of the spectroradiometer. For simulator 2, case 2 [Fig. 2(d)] correlation coefficients can be grouped into two main regions, the first up to 650 nm with similar coefficients as for simulator 1. The second region in the IR is less compact and additionally has correlation into the region below 600 nm.

This corresponds to Fig. 1, simulator 2, where the simulator light up to 650 nm is solely formed by the Xenon lamp, whereas light beyond 650 nm is a mix of overlapping Xenon and Halogen spectral irradiance.

The correlation coefficients matrices show the different influence on uncertainty, when using overlapping or separated light sources. For lowest uncertainty [Fig. 2(a), (c)] the correlation coefficients are also very low, and can become almost insignificant. For case 2 (calculations with higher uncertainty, [Fig. 2(b), (d)]), a significant difference between the two correlation coefficient matrices becomes visible. Two separate yellow blocks appear prominently, corresponding to the spectral bands of the two light sources. In a sensitivity analysis it has been noted, that the most responsive parameter is the irradiance instability of the light sources. The Xenon lamps fluctuate in irradiance independently of the Halogen lamps. This corresponds well to the block-like behavior of the correlation coefficients. As their spectral irradiance distributions overlap in different ways for the two solar simulators, also the distribution of correlation coefficients varies, and hence influences the uncertainty in measurement in different ways. As simulator 1 [Fig. 2(b)] has stronger spectral separation, also the coefficients form a clear block, whereas for simulator 2 the Halogen light is strongly superpositioned by the Xenon light. This corresponds well to the "dissolving" yellow block seen the in the plot [Fig. 2(d)].

In the following, we analyze the quantitative impact of simulator spectral design and reference solar cells on multi-junction cell calibration. As stated before, we can use the spectral mismatch factor for this comparison, as we keep all electrical and other hardware related uncertainties constant within the comparison. The uncertainty of the spectral mismatch for each subcell under test, therefore, gives insight into which spectral design has lowest

uncertainties in calibration with which respective reference solar cell.

The Monte Carlo simulation used for this analysis is based on the uncertainties listed in Table II (Appendix) and is calculated by (3) for 100.000 random draws for each combination of test subcell and reference cell. The results are listed in Table I. The mean value of all runs defines the respective spectral mismatch element SMM_{ij} of the matrix and is given in brackets. The standard deviation of all runs of the SMM_{ij} defines the relative uncertainty $u(SMM_{ij})$ and is presented as main values. Here, it is calculated with a coverage factor of $k = 2$, leading to a level of confidence of approximately 95 % [19].

Reference cells are categorized as "subcell adapted" (Ref007, 022 in Fig. 1) and "broadband" (Ref041, same Figure), and highlighted in color. The color highlighted fields correspond to meaningful combinations of subcell and reference cell. The lowest uncertainties in the comparison are reached for the subcell adapted reference cells. For simulator 1 this is very obvious. Although the mismatch factor is very close to unity for the broadband Ref041, the uncertainty is higher than for the subcell adapted reference cells. For simulator 2, the lowest uncertainty is again reached for the very well adapted reference Ref022 (bottom cell). Interestingly, the broadband Ref041 has a similar uncertainty as the combination of Ref007 and top cell. While Ref007 is illuminated almost only by Xenon light, the tested top cell is also receiving light from the Halogen lamp. The broadband Ref041 is subject to even more mixed light of Xenon and Halogen lamps. By chance, uncertainties for both combinations are similar. In addition, at simulator 2 the uncertainties for the broadband Ref041 are lower for both subcells, than for the same subcells calibrated at simulator 1. The reason is that both subcells are illuminated by both light sources, which results in lower uncertainties for the broadband device in contrast to a calibration at simulator 1, where both subcells receive light from (almost) one light source only.

Considering the relatively small value of this uncertainty contribution on the aforementioned $u(I_{sc}) = 1.5\ldots2$ %, it is important to mention that besides providing reproducible measurement, the main focus for calibration laboratories is to constantly reduce uncertainty in measurement, even if the effect is below 1 %.

In contrast, for measurements performed in regular laboratories, a multiple of the above stated uncertainties are present, and the effect of using a nonsubcell adapted reference has an even more pronounced impact. Depending on regular quality assessment and calibration routines even case 2 (Table III, Appendix) can be too optimistic.

B. Deviation of Device Uncertainty $u(I_{sc})$ from $u(I_{sc-TC, i})$ of the Limiting Subcell

The uncertainty of $I_{sc-TC,\ i}$ can be determined following (2). A series-connected multi-junction solar cell may have a device I_{sc} that deviates from the limiting subcell $I_{sc-TC,\ i}$. This deviation needs to be characterized to calculate the uncertainty $u(I_{sc-TC,\ device})$. As stated before, this effect can be caused by LC between the subcells, low R_p of the subcells or the RBB characteristic of the limiting subcell.

When setting the simulator to fulfill (1), each subcell will generate a current with an attributed uncertainty described by (2). The current mismatch of the multi-junction cell determines the degree of LC [13], and the reverse conditions under which the limiting subcell will operate. The influence of R_p on uncertainty of I_{sc} has been already discussed in [1]. In the following, we exclude the RBB from the analysis, as in practice it rarely occurs in solar cells sent to a calibration laboratory. However, as cell quality is constantly improving considering the influence from LC becomes increasingly important. Moreover, it has become a design criterion to increase radiative recombination and thus LC [31] between the subcells to increase efficiency and counter balance current mismatch.

LC and its influence on the calibration of multi-junction cells can be evaluated by different approaches. Detailed modeling with experimental fit parameters can be used on the one hand [13]. On the other hand, the influence of device current gain through radiative recombination by excess current of a higher or equal bandgap subcell can also be quantified by means of spectrometric characterizations [8], [15], [24], [32]. To illustrate the effects of LC on the device I_{sc} and its uncertainty, we evaluate two III–V dual-junction samples, where the epitaxial structure of the GaInP top cells has shown different radiative recombination, as seen in photoluminescence characterization (not shown here). *Sample 1* is a GaInP/GaAs (1.86 eV/1.42 eV) sample with a standard upright grown homo-junction GaInP top cell and GaAs bottom cell. *Sample 2* is a GaInP/AlGaAs (1.90 eV/1.48 eV) upright grown cell with a rear hetero GaInP top cell on an AlGaAs bottom cell (4.4 % Al). Although the samples were designed for the AM1.5d spectral irradiance, we use them here with AM1.5g, as a higher mismatch is possible with the respective solar simulator used.

In our assessment, we have set up a special spectrometric characterization (SMC) [24], where one of the subcells is set to generate the current it would at reference conditions, while only the other subcell is varied in current between $0.8\ldots1.2$ times its current at reference conditions. Hereby, we can evaluate the deviation from $I_{sc-TC,\ i}$, and hence $u(I_{sc-TC,\ device})$. The results of the SMC are plotted in Fig. 3 as measured test cell current in function of changing spectral conditions, given by the ratio of designated bottom cell current to designated bottom cell current at AM1.5g. Also plotted as open triangles are the calculated values for the current generated in the top and bottom cell, respectively, (based on the measured EQE). In the plots a) and b) the top cell current was kept constant at its values at AM1.5g, while the bottom cell current was varied.

Fig. 3(a) shows that for *sample 1* there is no measurable deviation of the device current from the calculated limiting subcell current derived from EQE characterization. At AM1.5g ($x = 1$) and for all x values below 1.1, the bottom cell is limiting the dual-junction solar cell. Deviations are in the range of uncertainty of fitting as shown in the upper plot of (a). The device current equals the current of the limiting subcell, the uncertainty of the device $u(I_{sc-TC,\ device})$ equals the uncertainty of the limiting subcell $u(I_{sc-TC,\ i})$.

For *sample 2,* the device current deviates distinctively from the calculated bottom cell current based on EQE measurement. As shown in the plot as a red line, the measured data can be fitted
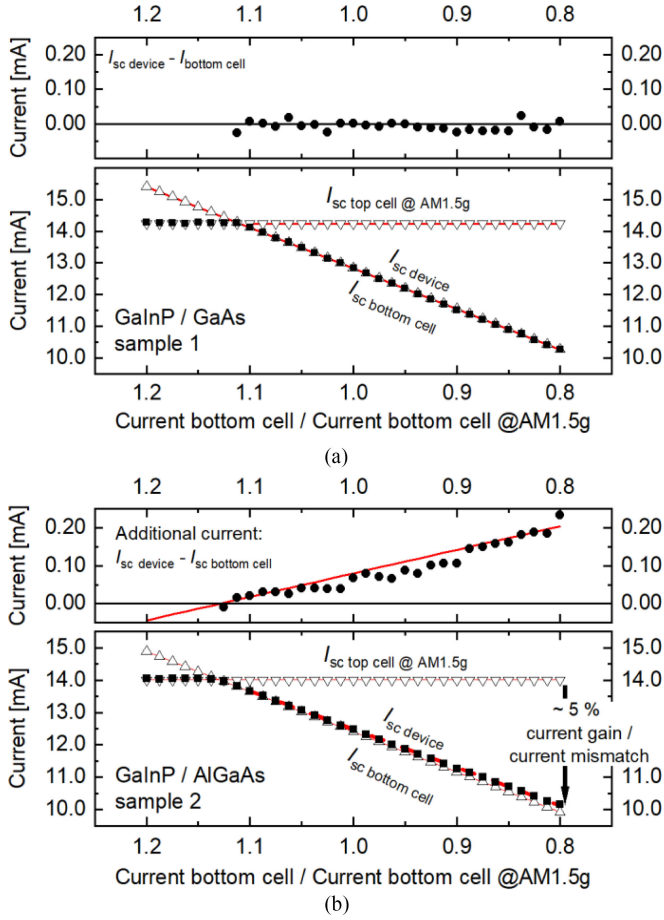
(a)

(b)

Fig. 3   Spectrometric characterization of two dual-junction GaInP/(Al)GaAs 1 cm² samples. Open triangles correspond to EQE based subcell currents. Solid squares show measured current, while solid circles show the delta between measured device and calculated bottom cell current.
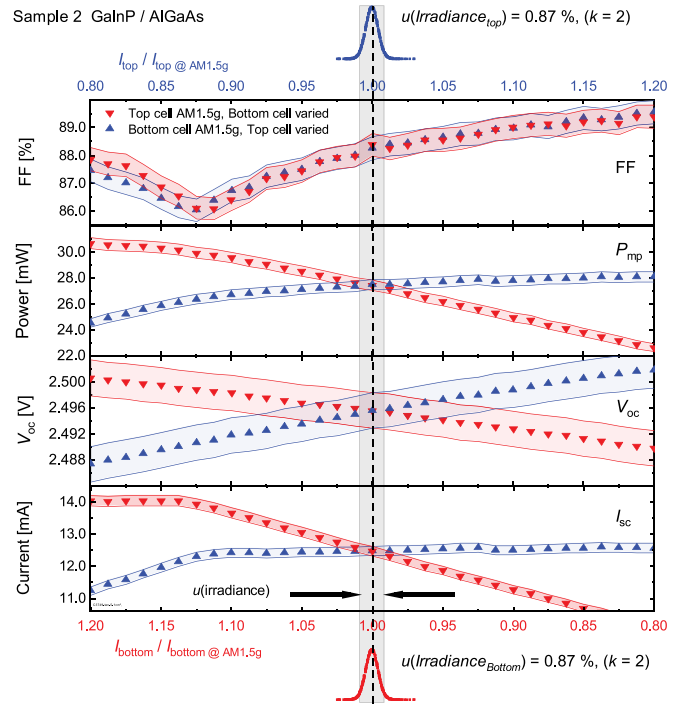

Fig. 4   Spectrometric characterization of the dual-junction GaInP/AlGaAs sample 2. Two distinct set of measurements are plotted: Red triangles, downward: variation of bottom cell current, while the top cell is constant at AM1.5g current. Blue triangles, upward: variation of top cell current, while the bottom cell is at constant AM1.5g current. The dashed line represents the data at AM 1.5g condition. Grey box: uncertainty of the irradiance on the subcells ($k = 2$).

well to an additional current of the bottom cell corresponding to 5 % of the current difference between top and bottom cell. The effect can be attributed to LC between the two subcells originating from electroluminescence caused by the excess current in the top cell.

The different results for the two samples can be explained with their radiative efficiencies which is thoroughly described elsewhere [33]. The influence of the observed current gain can be formulated in dependence of current mismatch for the device current (4). The experimentally derived equation matches suggestions found in literature for the case when effects in the dark current are negligible [34]. The uncertainty of the device short-circuit current $u(I_{sc-TC, device})$ can be formulated to (5) following the GUM. For *sample 2*, "*x*" equals 5.0 %. The uncertainty of the short-circuit current at AM1.5g spectral conditions for this sample depends mainly on the limiting bottom cell current and is influenced in small part by the uncertainty of the top cell current. The experimental method works well for high precision equipment. The determined percentages of current gain themselves come with uncertainty due to uncertainty of spectral irradiance, electrical measurement and other setup related factors. Please note that for reason of clarity these are

not shown in (5).

$$I_{sc} = I_{bottom} + x\,\% \left(I_{top} - I_{bottom}\right) \tag{4}$$

$$u(I_{sc}) = \sqrt{u\left((1 - x\,\%)\ I_{bottom}\right)^2 + u(x\,\% \left(I_{top}\right))^2} \tag{5}$$

C. Multi-Junction Device One Sun Efficiency Uncertainties

The spectrometric characterization method also allows for extraction of uncertainties of the other *I–V* parameters. Fig. 4 shows data for *sample 2* from the same measurements as described in Section B. Two sets of measurements were performed. For each spectral characterization one of the subcells was kept constant at its current at AM1.5g, while the other was varied by spectral settings of the solar simulator. E.g., the red downward triangles represent the measurement when the bottom cell current was varied and the top cell current was kept constant. The main *I–V* parameters are plotted in dependence of spectral settings expressed on the *x*-axis as ratio of the calculated subcell current to its current at reference conditions. The plot shows how the multi-junction sample reacts to changes in irradiance on subcell level and how this can be used to extract uncertainties of *I–V* parameters. At reference condition all subcells operate at $x = 1$. The uncertainty of irradiance for top and bottom cell set with the reference solar cell is equivalent to the input uncertainty of the metric, and is shown as grey underlying box. The two separate spectrometric measurements allow to distinguish the dependence on irradiance for each subcell individually. Datasets are attributed with uncertainties in *y*-direction shown as red and

blue uncertainty bands derived from electrical measurement, positioning, etc. The input uncertainty of the subcells (grey box) can be used to extrapolate the uncertainty of I–V parameters. As spectral uncertainty for both subcells needs to be considered, we include uncertainties obtained from the two spectrometric variations of top and bottom cell. With the maximum power as example parameter we can formulate:

$$u\left(P_{\mathrm{mp}}\right) = \sqrt{\left(u\left(P_{\mathrm{mp,top-var}}\right)\right)^2 + \left(u\left(P_{\mathrm{mp,bot-var}}\right)\right)^2}. \quad (6)$$

Finally, the uncertainty for the efficiency can be determined, by combining the uncertainty of measured maximum power and the uncertainty of the solar cell area measurement. For the specific *sample 2* this results in $U(\eta) = 2.59\,\%$ ($k = 2$).

The analytical derivation shown above is an approach that in future work will be compared with a Monte Carlo simulation, accounting also for correlation of uncertainties.

To illustrate the method we have used a simple dual-junction cell. Obviously, also devices with more junctions can be evaluated, where optical coupling may occur between several subcells. Instead of performing all possible SMC permutations, it can be decided for relevant measurement combinations to limit measurement time.

III. CONCLUSION

Detailed literature on the uncertainty of multi-junction solar cell characterization is scarce. For the example of dual-junction solar cells a general method tracing the calibration chain in the electrical I–V characterization to international metrological standards has been introduced.

One priority of this article is to evaluate the influence of solar simulator spectral irradiance distributions and reference solar cells on measurement uncertainty. Two simulators with separated and overlapping lamp spectral irradiances were assessed for a perovskite/silicon tandem device (Oxford PV/Oxford/Helmholtz) [23] considering broadband and subcell adapted reference cells. With a Monte Carlo approach we accounted for uncertainty components including wavelength dependent correlations. The measurement uncertainty of the respective spectral mismatch (SMM_{ij}) was found to be generally lower if a subcell adapted reference cell was used. For the solar simulator with overlapping spectral irradiance distributions the broadband reference solar cell can produce similar uncertainties as the subcell adapted.

In the other main area of this article, we use a spectrometric characterization method to determine the uncertainty of the short-circuit current of a multi-junction solar cell including the influence of electroluminescent coupling. With the same spectrometric characterization, the uncertainties of the other I–V parameters can be obtained. An expanded uncertainty ($k = 2$) of 2.59% for efficiency for the specific 1 cm² test cell can thereby be reached at present at CalLab PV Cells (Fraunhofer ISE).

Please note that the calculated uncertainties of the specific cell are a consequence of very low uncertainties of the input parameters measured with highly sophisticated setups and procedures that require constant and thorough review, as is done by accredited calibration laboratories. For laboratory measurements which do not meet the above mentioned requirements and which do not rigorously re-evaluate their equipment constantly, these uncertainty values can easily become a multiple of the above stated.

APPENDIX

We use the appendix to show additional information on the Monte Carlo simulation. Table II lists the wavelength correlated uncertainties. As described in the text (Section II, A) we have set up a case 2 scenario to compare the results for the equipment in use in our laboratory (case 1) to less advanced equipment. The values for case 1 are based on decade long experience with the equipment in use. For case 2, we had to refer to datasheet values of a Zeiss spectroradiometer, and for irradiance instabilities we decided for the A+ requirements of the new standard [30]. The results for the case 2 uncertainties of the spectral mismatch factor matrix $u(SMM_{ii})$ can be found in Table III.

In difference to the IEEE paper [1] we have enlarged the statistical significance to 100.000 Monte-Carlo draws and have

TABLE II
INPUT UNCERTAINTIES FOR THE MONTE CARLO SIMULATION

Solar Simulator Spectra:			
Uncertainty	Case 1	Case 2	type
Irradiance	0.3 %	1 %	rel., wavelength correlated
Bandwidth	3 nm	4 nm	abs., wavelength correlated
Wavelength	0.1 nm	0.2 nm	abs., wavelength correlated
Irradiance, etc.	0.5 %	0.5 %	rel., range correlated (100 nm)
And other uncorrelated uncertainties			
Test and Reference Spectral Responsivity:			
50% rel. wavelength correlated and			

Wavelength correlated uncertainty components for the calculation of the Monte Carlo simulation of the spectral mismatch matrix ($k = 2$). The assumptions for case 1 are realistic only for highly sophisticated setups in calibration laboratories with thoroughly reviewed and constantly monitored procedures. For case 2 industrial grade spectroradiometer, irradiance instability: Class A+ simulator, and thoroughly reviewed and constantly monitored procedures are considered.

TABLE III
UNCERTAINTY MATRIX OF THE SPECTRAL MISMATCH – CASE 2

Solar Simulator 1	**Reference Cells**		
	Subcell adapted		**Broadband**
	Ref007	Ref022	Ref041
Perovskite Top	0.23 % (1.0037)	1.39 % (0.9753)	0.63 % (0.9990)
Silicon Bottom	1.33 % (1.0036)	0.18 % (0.9752)	0.63 % (0.9989)

Solar Simulator 2	**Reference Cells**		
	Subcell adapted		**Broadband**
	Ref007	Ref022	Ref041
Perovskite Top	0.39 % (1.1795)	0.81 % (1.0528)	0.36 % (1.0083)
Silicon Bottom	1.05 % (1.1794)	0.14 % (1.0526)	0.38 % (1.0082)

Case 2. Relative uncertainties of the spectral mismatch $u(SMM_{ij})$ for the dual-junction perovskite/silicon test device (Oxford PV/Oxford/Helmholtz) and the subcell adapted and broadband reference cells at both solar simulators. The spectral mismatch value SMM_{ij} is given in brackets. 100.000 Monte Carlo draws. Reference cells named according to Fig. 1.

introduced a Gaussian distribution for range correlated uncertainties. The simulation was programmed in Python.

REFERENCES

[1] S. K. Reichmuth *et al.*, "Measurement uncertainties in the calibration of multi-junction devices for different sun simulators and reference devices," in *Proc. Conf. Rec. 46th Photovolt. Specialists Conf.*, Chicago, USA, 2019, pp. 0082–0086.

[2] A. Richter, M. Hermle, and S. W. Glunz, "Reassessment of the limiting efficiency for crystalline silicon solar cells," *IEEE J. Photovolt.*, vol. 3, no. 4, pp. 1184–1191, Oct. 2013.

[3] R. Cariou *et al.*, "III–V-on-silicon solar cells reaching 33% photoconversion efficiency in two-terminal configuration," *Nature Energy*, vol. 17, 2018, Art. no. 183.

[4] H. J. Snaith, "Present status and future prospects of perovskite photovoltaics," *Nature Mater.*, vol. 17, no. 5, pp. 372–376, 2018.

[5] M. A. Green *et al.*, "Solar cell efficiency tables (version 54)," *Prog. Photovolt., Res. Appl.*, vol. 27, no. 7, pp. 565–575, 2019.

[6] *General requirements for the competence of testing and calibration laboratories*, ISO/IEC 17025, 2017.

[7] C. R. Osterwald *et al.*, "The world photovoltaic scale: An international reference cell calibration program," *Prog. Photovolt., Res. Appl.*, vol. 7, no. 4, pp. 287–297, 1999.

[8] M. Meusel, R. Adelhelm, F. Dimroth, A. W. Bett, and W. Warta, "Spectral mismatch correction and spectrometric characterization of monolithic III-V multi-junction solar cells," in *Proc. Progr. Photovolt., Vol.10 (2002), No.4, N-17060*, 2002, pp. 243–255.

[9] *Handbook of Concentrator Photovoltaic Technology*. Hoboken, NJ, USA:Wiley, 2016.

[10] D. J. Friedman, J. F. Geisz, and M. A. Steiner, "Analysis of multijunction solar cell current–voltage characteristics in the presence of luminescent coupling," *IEEE J. Photovolt.*, vol. 3, no. 4, pp. 1429–1436, Oct. 2013.

[11] S. K. Reichmuth *et al.*, "On the temperature dependence of dual-junction laser power converters," *Prog. Photovolt., Res. Appl.*, vol. 25, no. 1, pp. 67–75, 2017.

[12] A. Braun *et al.*, "Current-limiting behavior in multijunction solar cells," *Appl. Phys. Lett.*, vol. 98, no. 22, 2011, Art. no. 223506.

[13] J. F. Geisz *et al.*, "Generalized optoelectronic model of series-connected multijunction solar cells," *IEEE J. Photovolt.*, vol. 5, no. 6, pp. 1827–1839, Nov. 2015.

[14] K. Emery *et al.*, "Procedures for evaluating multijunction concentrators," in *Conf. Record 28th IEEE Photovolt. Specialists Conf.*, Anchorage, Alaska, USA, 2000, pp. 1126–1130.

[15] C. R. Osterwald and G. Siefer, "CPV multijunction solar cell characterization in," *Handbook of Concentrator Photovoltaic Technology*. Hoboken, NJ, USA: Wiley, 2016, pp. 589–614.

[16] R. Timmreck *et al.*, "Characterization of tandem organic solar cells," *Nature Photon.*, vol. 9, no. 8, 2015, Art. no. 478.

[17] Y. Hishikawa, "Characterization of the silicon-based thin film multijunction solar cells," *MRS Proc.*, vol. 862, 2005, Art. no. 1126.

[18] T. Glatfelter and J. Burdick, "A method for determining the conversion efficiency of multiple-cell photovoltaic devices," in *Conf. Record 19th IEEE Photovolt. Specialists Conf.*, New Orleans, LA, USA, 1987, pp. 1187–1193.

[19] *Guide to the Expression of Uncertainty in Measurement*, BIPM, IEC, IFCC, ILAC, ISO, IUPAP and OIML, JCGM 100, 1995.

[20] *Photovoltaic devices - Part 7*, IEC 60904-7, 2008.

[21] C. H. Seaman, "Calibration of solar cells by the reference cell method—The spectral mismatch problem," *Solar Energy*, vol. 29, no. 4, pp. 291–298, 1982.

[22] J. Hohl-Ebinger and W. Warta, "Uncertainty of the spectral mismatch correction factor in STC measurements on photovoltaic devices," *Prog. Photovolt., Res. Appl.*, vol. 19, no. 5, pp. 573–579, 2011.

[23] M. A. Green *et al.*, "Solar cell efficiency tables (version 52)," *Prog. Photovolt., Res. Appl.*, vol. 26, no. 7, pp. 427–436, 2018.

[24] C. Baur and A. W. Bett, "Measurement uncertainties of the calibration of multi-junction solar cells," in *Conf. Record 31st IEEE Photovolt. Specialists Conf.*, Orlando, Florida, USA, 2005, pp. 583–586.

[25] H. Field and K. Emery, "An uncertainty analysis of the spectral correction factor," in *Conf. Record 23rd IEEE Photovolt. Specialists Conf.*, Louisville, KY, USA, 1993, pp. 1180–1187.

[26] K. D. Sommer and B. R. L. Siebert, "Systematic approach to the modelling of measurements for uncertainty evaluation," *Metrologia*, vol. 43, no. 4, 2006, Art. no. S200.

[27] R. Kacker, K.-D. Sommer, and R. Kessel, "Evolution of modern approaches to express uncertainty in measurement," *Metrologia*, vol. 44, no. 6, pp. 513–529, 2007.

[28] S. Winter and A. Sperling, "Uncertainty analysis of a photometer calibration at the DSR setup of the PTB," in *Proc. 2nd Expert Symp. Meas. Uncertainty, Braunschweig*, 2006, pp. 139–142.

[29] *Photovoltaic devices - Part 3*, IEC 60904-3, 2008.

[30] *Photovoltaic devices - Part 9*, DIN EN 60904-9:2018-04, 2018.

[31] M. Wilkins *et al.*, "Luminescent coupling in planar opto-electronic devices," *J. Appl. Phys.*, vol. 118, no. 14, 2015, Art. no. 143102.

[32] A. J. Bett *et al.*, "Two-terminal Perovskite silicon tandem solar cells with a high-Bandgap Perovskite absorber enabling voltages over 1.8 V," *Prog. Photovolt., Res. Appl.*, vol. 2, no. 5, 2019, Art. no. 17032.

[33] J. F. Geisz *et al.*, "Enhanced external radiative efficiency for 20.8% efficient single-junction GaInP solar cells," *Appl. Phys. Lett.*, vol. 103, no. 4, 2013, Art. no. 41118.

[34] M. A. Steiner et al., "Measuring IV curves and subcell photocurrents in the presence of luminescent coupling," *IEEE J. Photovolt.*, vol. 3, no. 2, pp. 879–887, Apr. 2013.